Designing photocured macromolecular matrices for stable potassium batteries

Designing photocured macromolecular matrices for stable potassium batteries

Matteo Gandolfo,[1] Julia Amici,[1,2*] Lucia Fagiolari,[1,2] Carlotta Francia,[1,2] Silvia Bodoardo,[1,2] Federico Bella[1,2*]

[1] Department of Applied Science and Technology, Politecnico di Torino, Corso Duca degli Abruzzi 24, 10129 – Torino, Italy

[2] National Interuniversity Consortium of Material Science and Technology (INSTM), Via Giuseppe Giusti 9, 50121 – Firenze, Italy

Corresponding authors: federico.bella@polito.it; julia.amici@polito.it

Designing photocured macromolecular matrices for stable potassium batteries

Keywords: Potassium batteries; Polymer electrolyte; UV-curing; Photopolymerization; Post-lithium batteries.

Abstract: The preparation and characterization of the first photocured gel polymer electrolyte for potassium batteries is presented. The use of UV-induced radical polymerization aims at developing a sustainable and rapid way to produce polymer electrolytes without using further processes to separate solvents and by-products. The gel polymer electrolyte displays a high ionic conductivity (17 mS cm^{-1} at 20 °C) and an electrochemical stability window up to 3.7 V (*vs.* K^+/K), maintaining excellent stability within battery working potential range. The thermal resistance is suitable for potassium battery application and the glass transition temperature is low enough to ensure a good macromolecular mobility of the polymer chains. Due to the highly crosslinked structure, the gel polymer electrolyte is mechanically robust and able to hinder the formation of potassium dendrites, i.e. one of the main issue to be faced for this energy storage technology, allowing the unprecedented achievement of 600 cycles with a capacity retention of 58%.

1. Introduction

Global warming is a growing problem in our society and an important reduction in greenhouse gas emissions is necessary to mitigate the effects of climate change [1,2,3]. Renewable sources, like photovoltaic and wind power plants, can be exploited to produce energy with less emissions, but with intermittency during days and seasons [4,5,6]. For this reason, stationary energy storage technologies are necessary to stabilize the grid and supply energy when needed [7,8,9,10,11]. Currently adopted energy storage technology is mainly based on the lithium-ion battery (LIB) concept, that has gained wide success in the last decades [12,13,14,15]. LIBs, owing to high energy density and high operative voltage, are widely used in portable electronics and electric vehicles [16,17,18]. However, lithium is

a scarce resource with uneven distribution on Earth [19,20,21] and its increasing cost limits the development of large-scale energy storage based on LIBs [22,23,24]. Therefore, new elements are now investigated by the scientific community [25,26].

Sodium-ion batteries (SIBs) and potassium-ion batteries (KIBs) are promising alternatives of LIBs due to their alkali metal high abundance (2.09 wt% for potassium and 2.36 wt% for sodium) and homogeneous distribution on the Earth crust [27,28,29,30,31]. The first KIB prototype was developed in 2004 by Eftekhari [32]; in the subsequent years, potassium received less attention than sodium, but this element presents some peculiar features that are pushing ahead the activity of many research groups. Indeed, the redox potential of K^+/K (–2.91 V *vs.* standard hydrogen electrode (SHE)) is much closer to that of Li^+/Li (–3.04 V *vs.* SHE) with respect to that of Na^+/Na (–2.71 V *vs.* SHE). In the meantime, when working with carbonate solvents, potassium presents a lower standard potential than lithium, as it occurs in an ethylene carbonate (EC)/diethylene carbonate (DEC) mixture (–0.12 V *vs.* Li^+/Li), overall providing higher energy density [29,33]. Even though the largest ionic radius belongs to K^+, it shows a lower Lewis acidity that brings this ion to possess the lowest Stokes' radius in propylene carbonate when compared to Li^+ and Na^+ [34]. Hence, the weak Lewis acidity and desolvation energy of K^+ permit the achievement of higher rate capability [35]. Another important difference from LIBs is the possibility to use aluminium as a current collector for both anode and cathode side, with important cost and weight reduction; this is possible considering that no alloying reaction between potassium and aluminium has been reported [33]. Moreover, as for LIBs, K^+ can intercalate in graphite forming KC_8 compound with a theoretical capacity of 280 mAh g^{-1}, while scarce results are reached with the same anode in SIBs [36].

As regards KIBs current drawbacks, one important issue is that potassium shows a lower melting point and stronger reactivity than other alkali metals, thus dendrite growth is a crucial safety concern [34]. This affects the choice of the electrolyte system. It is well known that liquid electrolytes are highly ionically conductive and present a good contact with the electrodes, but they are at the same time flammable, prone to leak and not able to suppress dendrite growth. Due to these issues, gel

polymer electrolytes (GPEs) have been investigated in recent years to replace liquid counterparts and – in our opinion – seem the most reasonable choice for KIBs. GPEs combine the advantages of both liquid and solid electrolytes, they ensure good mechanical properties and flexibility, but also high conductivity and good interfacial contact with electrodes [37,38,39,40]. Probably because KIB represents a recent technology, very few studies have been published on polymer-based electrolytes for K^+ conduction. Goodenough *et al.* studied a crosslinked poly(methyl methacrylate) GPE that was able to suppress dendrite growth [27]. It showed an ionic conductivity of 4.3×10^{-3} S cm^{-1} at room temperature and a stability up to 4.9 V *vs.* K^+/K; the galvanostatic charge/discharge test evidenced a capacity retention of 98% after 100 cycles at current density of 50 mA g^{-1}. Feng *et al.* developed an all-solid-state KIB based on an organic cathode and a solid polymer electrolyte, the latter consisting of poly(propylene carbonate) with cellulose nonwoven backbone [41]. A ionic conductivity of 1.36×10^{-5} S cm^{-1} at 20 °C was achieved and the resulting half-cell delivered an initial capacity of 118 mAh g^{-1} at 10 mA g^{-1}. A single ion-conducting electrolyte based on dimethoxyethane-swollen poly((trifluoromethyl)sulfonyl) (4-vinylphenyl) amide (KPSTFSA) with Al_2O_3 as a filler was developed by Wu *et al.* [42]. This GPE showed a high ionic conductivity (6.0×10^{-2} S cm^{-1} at 20 °C) and a high K^+ transference number (0.87), but it decomposed showing that the poly(styrene) structure of KPSTFSA was unstable for KIB application.

In this work, we present the first UV-cured electrolyte for KIBs, obtained by the free-radical copolymerization of butyl methacrylate (BMA) and poly(ethylene glycol) diacrylate (PEGDA). Photopolymerization is a sustainable and energy saving technique, prone to upscale the production, used to prepare crosslinked polymeric films starting from the monomers mixture in a rapid manner without using solvents and catalysts [43]. Two different strategies are here investigated for GPEs preparation. The first one consists in the preparation of a precursor solution (BMA, PEGDA and photoinitiator) with a small quantity of EC, used as plasticizer, subsequently UV-cured and activated by swelling into a liquid electrolyte. The second strategy is based on the preparation of a precursor solution already containing the K^+-based liquid electrolyte. Both GPEs expressed a high ionic

conductivity of 1.7×10^{-2} S cm^{-1} at 20 °C. Interestingly, the GPE obtained by UV-curing the liquid electrolyte-laden formulation was able to efficiently limit dendrites growth, enabling to reach up to 600 cycles in lab-scale prototypes with a 58% capacity retention at 0.05 A g^{-1}; as a comparison, a standard cell cycled under similar conditions failed after approximately 210 cycles.

2. Material and Methods

2.1 Materials

BMA was purchased from Acros Organics. PEGDA (average M_n 575), 2-hydroxy-2-methylpropiophenone (Darocur® 1173), potassium (98%), EC, DEC, 1-methyl-2-pyrrolidone (NMP) and potassium hexafluorophosphate (KPF_6) were supplied by Sigma-Aldrich. Carbon black Super-P was purchased from Alfa Aesar, while poly(vinylidene difluoride) (PVDF) as polymer binder (HSV 900:ADX 160 90:10 wt.%) was acquired from Arkema. The non-aqueous liquid electrolyte was based on KPF_6 0.80 M in a EC:DEC mixture (1:1 *v/v*). Each electrochemical characterization shown in this work for the newly designed GPE was compared to the result given by a reference cell containing a glass fiber separator (Whatman®) soaked with the same liquid electrolyte and referred to as "standard cell".

2.2 Membranes and electrodes preparation

Polymer membranes were obtained by UV-induced free radical polymerization. Two different formulations were prepared, *i.e.* 70/20/10 and 70/20/10+KPF_6, both containing BMA 70 wt% and PEGDA 20 wt%; the first mixture contained EC 10 wt%, while the second one included 10 wt% of liquid electrolyte. The formulations were prepared in an argon-filled glove box (Mbraun Labstar, O_2 and H_2O contents <0.5 ppm), vigorously mixed and sandwiched between two microscope plates separated by a 200 µm-thick spacer. Radical polymerization occurred under UV radiation from a high-intensity mercury-xenon lamp (Lightning Cure LC8, Hamamatsu) for 7 min. Before assembling

electrochemical cells, the membranes were quickly activated by swelling in the organic-liquid electrolyte.

When assembling half-cells, the active electrode was prepared starting from a 80:20 ratio between powders of conductive carbon black Super P and PVDF as polymer binder; they were mixed in NMP. The as-obtained slurry was evenly deposited on a 10 µm-thick copper foil with a 200 µm-thick doctor blade and dried in the oven for 90 min at 50 °C; the mass loading was 0.72 mg cm^{-2}. Electrodes were cut in discs with a diameter of 15 mm, vacuum-dried and stored in an argon-filled glove box (LABmaster Pro, MBRAUN).

2.3 Characterization techniques

Field-emission scanning electron microscopy (FESEM) Tescan S9000G was used to observe membranes surface and cross-section.

X-rays diffraction (XRD) was performed with a high-resolution Philips X'pert MPD powder diffractometer, equipped with Cu Kα radiation (V = 40 kV, I = 30 mA) and a curved graphite secondary monochromator; polymer membranes were characterized to assess their macromolecular structure and confirm the presence of KPF_6 salt in the 70/20/10+KPF_6 formulation. The diffraction profiles were collected in the 2θ range between 15° and 90°, with an acquisition step of 0.018° and a time per step of 10 s using a solid-state PIXcel-1D detector with 255 active channels.

Samples thermal stability was measured by thermogravimetric analysis (TGA) between 25 and 800 °C, at a heating rate of 10 °C min^{-1} under N_2 flux. TGA was performed with a TG 209 F3 Tarsus instrument by Netzsch. Differential scanning calorimetry (DSC) was carried out to determine the glass-transition temperature (T_g) and the crystallinity fraction of polymer electrolyte (X_c) by measuring the melting enthalpy ($\Delta H_m(T_m)$) and comparing it with the melting enthalpy of a fully crystalline polymer ($\Delta H_m^0(T_m^0)$). DSC was carried-out with Mettler Toledo equipment, working between –90 and 250 °C at a heating rate of 10 °C min^{-1} under N_2 flux.

The ionic conductivity (σ) was evaluated by VSP-3e potentiostat (Biologic), carrying out electrochemical impedance spectroscopy (EIS) in the frequency range between 1 Hz and 100 KHz with an amplitude of 10 mV at the open-circuit potential. The measurement was conducted on a symmetric cell consisting of the electrolyte sandwiched between two stainless steel (SS) blocking electrodes in ECC-Std test cells (EL-CELL GmbH). Tests were carried out in a dynamic climate chamber (MKF 56, Binder) at intervals of 10 °C in the range 10-60 °C. Ionic conductivity values measured at different temperatures were calculated following **Equation 1**:

$$\sigma = \left(\frac{l}{A}\right) \cdot \left(\frac{1}{R_s}\right) \qquad (1)$$

where l is the membrane thickness, A is the membrane surface area and R_s is the resistance value at the high-frequency intercept. The obtained results, plotted versus 1000/T (K), were then fitted with the Arrhenius' relationship shown in **Equation 2**:

$$\sigma = \sigma_0 \cdot e^{-\frac{E_a}{kT}} \qquad (2)$$

where E_a is the activation energy, k is the Boltzmann's constant and T is the test temperature.

The interfacial stability of GPEs in contact with potassium metal electrodes was established by carrying out EIS in the frequency range between 100 kHz and 1 Hz, at open circuit potential, at regular time intervals on symmetric coin cell (CR 2032) consisting of gel polymer electrolytes sandwiched between two potassium metal electrodes. Symmetric cells were tested by CHI660D electrochemical workstation and stored at open circuit potential at room temperature.

The ability of the electrolytes to suppress the growth of potassium dendrites was evaluated according to the method developed by Goodenough *et al.* [27], consisting of a galvanostatic polarization of a potassium symmetric cell. The test was carried out by continuously plating one electrode at a fixed current density (0.1 mA cm^{-2}). The time necessary to short-circuit the cell can be compared to that of standard cell, proving the ability of newly developed GPEs to suppress the growth of potassium dendrites.

Galvanostatic charge and discharge cycle were also carried out on a symmetrical ECC-Std cell to assess the polymer electrolyte performance through a continuous plating and stripping test. The

electrochemical cell was subjected to charge and discharge for 1 h at a current density of 0.05 mA cm^{-2} for 50 cycles and then at a current density of 0.1 mA cm^{-2} for further 50 cycles. The test was carried out on an Arbin BT-2000 battery tester

The electrochemical stability window was measured by linear sweep voltammetry (LSV) using CHI660D potentiostat. The cell, assembled sandwiching the GPE between a potassium metal electrode and a SS blocking electrode, was tested in the 1-5 V range under a scan rate of 0.1 mV s^{-1} at room temperature.

Cyclic voltammetry (CV) was carried out to characterize the electrochemical reactions occurring in a cell assembled with potassium metal as a counter electrode, conductive carbon black Super P as working electrode and the GPE (referred to, from now on, as half-cell setup), within 0.01-3 V operative potential at a scan rate of 0.1 mV s^{-1}, working with a the VSP-3e potentiostat at room temperature.

Galvanostatic charge/discharge tests were carried out to evaluate the electrochemical performance of GPEs-based KIB prototypes in comparison with a standard cell. The half-cells were subjected to different current densities ranging from 0.05 A g^{-1} to 1 A g^{-1} at ambient temperature in the ECC-Std cell with an Arbin BT-2000 battery tester.

3. Results and Discussion

Two different GPEs prepared by photopolymerization were investigated for KIBs. Both formulations were composed of BMA monomer and PEGDA crosslinker in a 70:20 ratio, allowing the obtainment of a highly crosslinked polymeric matrix. Two different formulation strategies were studied: the first one was based on the addition of EC 10 wt% in the reactive mixture (the corresponding sample is referred to as 70/20/10), while the second approach was based on the introduction of 10 wt% of liquid electrolyte (KPF_6 0.80 M in EC:DEC (1:1 *v/v*)) to the formulation (referred to as 70/20/10+KPF_6). After a 7 min photopolymerization step, the two formulations were visually similar, transparent, not

sticky and mechanically robust. Furthermore, the activated GPEs were self-standing, flexible and easy to handle, as shown in **Figure 1AB**.

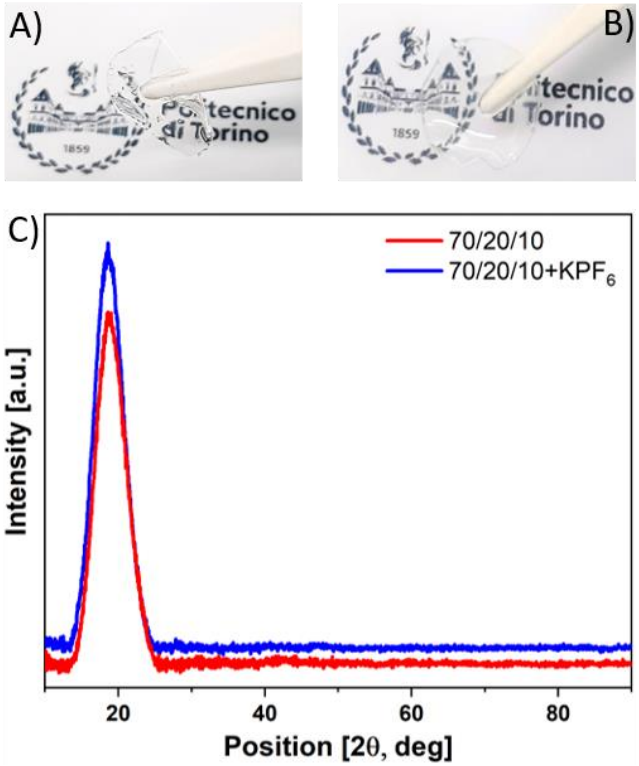

Figure 1 Photograph of A) 70/20/10+KPF_6 and B) 70/20/10 electrolytes after the activation process; C) XRD pattern of 70/20/10 and 70/20/10+KPF_6 electrolytes. Of note, the XRD pattern intensity of KFP_6 has been halved for graphical reasons.

The morphology of the membranes was obtained by FESEM study and the micrographs are shown in **Figure S1**. The surface of the 70/20/10+KPF_6 electrolyte was corrugated and the cross-section was smooth and dense, with a thickness of about 170 µm. The 70/20/10 electrolyte also presented a wave-like surface, but the cross-section was less dense and much more irregular, with a thickness of around 170 µm.

The crystallinity of a polymer used as a GPE can be a great obstacle for ions conduction [44,45], therefore XRD analysis was carried out on the prepared samples and the corresponding patterns are reported in **Figure 1C**. The diffractograms revealed – for both formulations – an amorphous peak at $2\theta = 18.7°$, indicating the absence of a crystalline phase into the polymer matrix.

In the meantime, X_c and T_g were assessed by DSC analysis under N_2 flow, to verify the absence of crystallinity detected by XRD study. Due to heat-capacity variation, T_g identified in the point of slope change of DSC curves was –52 °C for 70/20/10 sample and –47 °C for 70/20/10+KPF_6 system, as shown in **Figure 2**. These values are sufficiently low to ensure good macromolecular mobility of polymer chains and proper elasticity of the membrane at room temperature. DSC curves, shown in **Figure 2**, presented no endothermic peaks between 30 °C and 250 °C, indicating the absence of crystallinity domain in both formulations, while – according to the literature [46] – pristine PEO has a melting temperature of 72.9 °C. Although in GPEs ions conduction occurs principally in the liquid electrolyte incorporated in the polymer matrix [46], the absence of crystallinity and good mechanical properties are widely recognized as optimal features for polymer electrolytes [47].

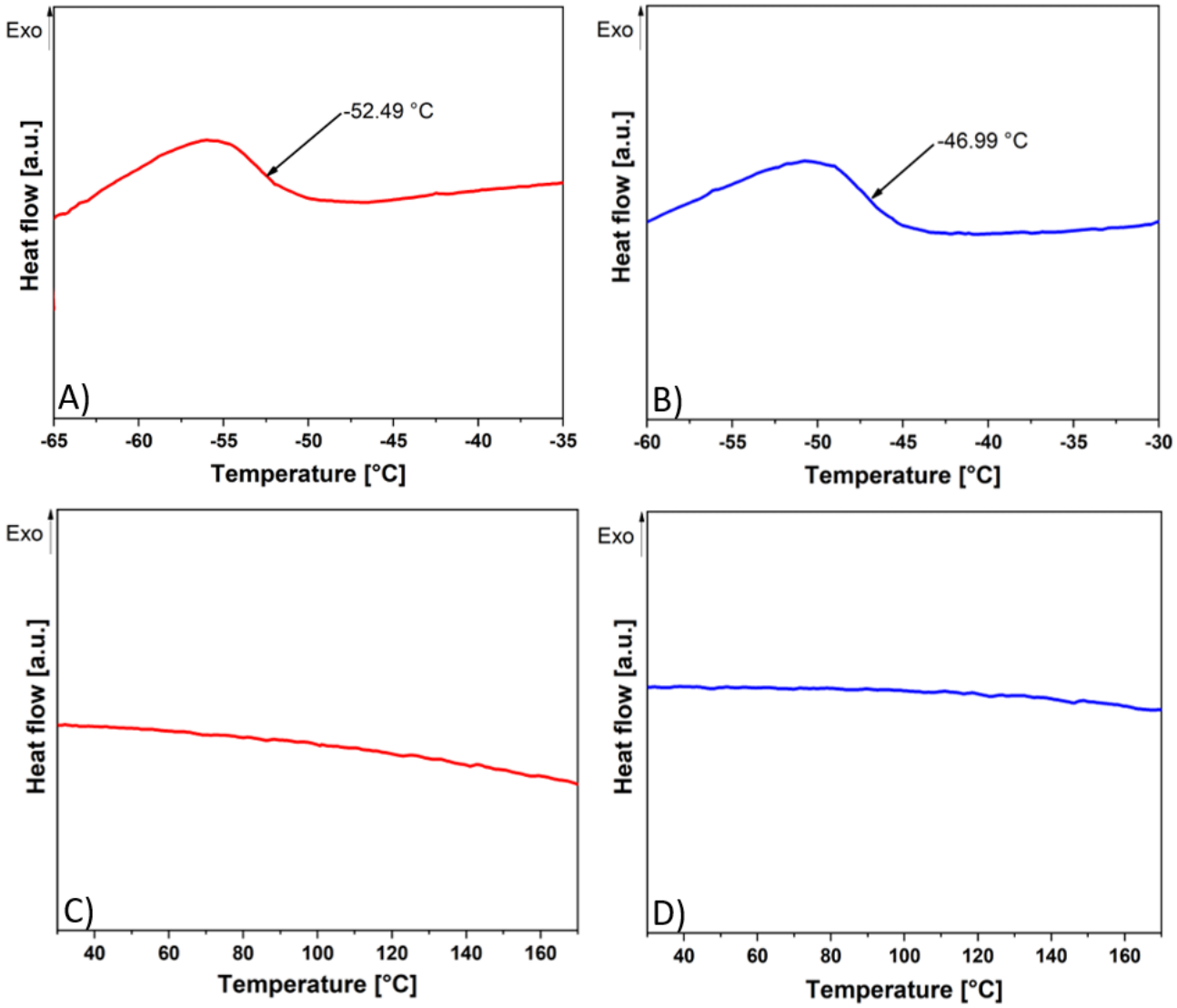

Figure 2 DSC analysis (10 °C min^{-1}, N_2 atmosphere) of A,C) 70/20/10 electrolyte and B,D) 70/20/10+KPF_6 electrolyte.

The thermal stability of the polymer electrolytes was assessed by TGA under N_2 flow between 25 and 800 °C. Two principal degradation pathways were clear in the resulting TGA traces, as reported in **Figure 3AB**. Both GPEs were thermally stable up to 200 °C, then they underwent thermal degradation with two maximum degradation rates at 282/385 and 275/375 °C for 70/20/10 and 70/20/10+KPF_6 samples, respectively. This behaviour can be partially ascribed to the evaporation – at a temperature over 100 °C – of the plasticizer added in the reactive mixture, as shown in **Figure 3C**, but it is principally caused by polymer backbone degradation. Degradation residue at 500 °C was 0.18% for 70/20/10 sample and 3.3% for 70/20/10+KPF_6 system. This trend can be explained by the presence of salt in the 70/20/10+KPF_6 sample, starting to decompose at 450 °C, as shown in **Figure**

3C, and only partially decomposed at 500 °C. The two polymer electrolytes substantially followed the same thermal degradation pathway. The first step localized between 160 and 210 °C was due to the evaporation of low molecular weight like solvents, residual monomers and oligomers. The second step of thermal degradation between 240 and 280 °C could be ascribed to the scission of C–C bonds in β to the vinyl group, causing the depolymerization of the methacrylate fraction. The last and final step between 320 and 380 °C indicated the degradation of the remaining polyether backbone [48,49,50]. According to TGA analysis, both formulations present adequate thermal stability for KIBs applications.

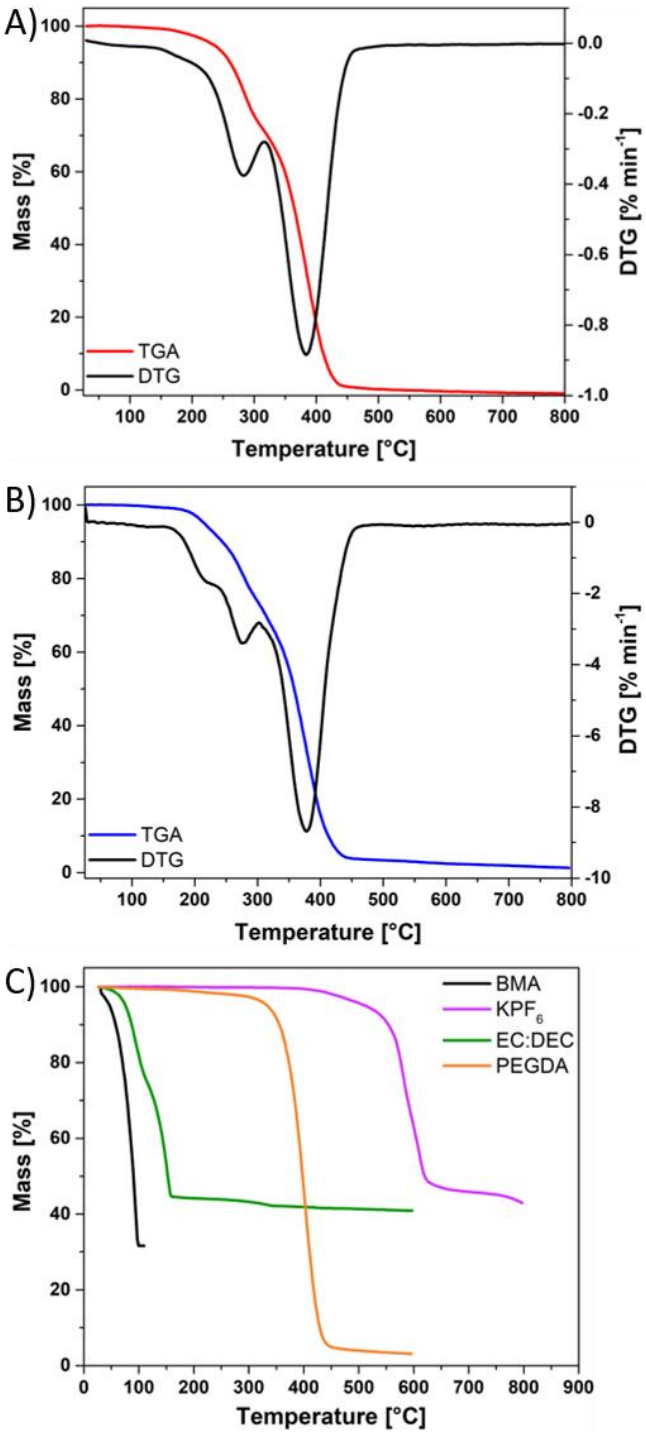

Figure 3 TGA analysis (10 °C min^{-1}, N_2 atmosphere) of A) 70/20/10 electrolyte, B) 70/20/10+KPF_6 electrolyte, C) individual components of the formulations (*i.e.*, BMA, KPF_6, EC:DEC and PEGDA).

An in-depth electrochemical characterization was set to investigate the performance of the UV-cured polymer membranes in KIBs. The σ was assessed by EIS at different temperatures (in the 10-60 °C range). Cells were assembled with the two different GPEs sandwiched between two blocking SS electrodes in ECC-Std configuration. The outcome of this study is summarized in **Figure 4**. Both

membranes demonstrated σ values of 0.017 S cm^{-1} at 20 °C, this latter representing an outstanding achievement when compared to the state of the art [51]; when tested at 60 °C, the 70/20/10 electrolyte reached a value of 0.032 S cm^{-1}, higher than that (0.025 S cm^{-1}) achieved by the 70/20/10+KPF_6 sample. σ values in the explored temperature range were fitted by Arrhenius' relationship and E_a values were calculated. The 70/20/10 electrolyte showed an E_a of 13.1 kJ mol^{-1}, while the 70/20/10+KPF_6 one featured a slightly lower E_a, *i.e.* 8.42 kJ mol^{-1}. The two polymer electrolyte formulations obtained quite good results with limited differences in the side points of the explored temperature interval. Cations mobility at low temperature could also be favoured by the higher presence of DEC in the 70/20/10+KPF_6 electrolyte, since DEC is a linear molecule featuring a lower viscosity than EC [52].

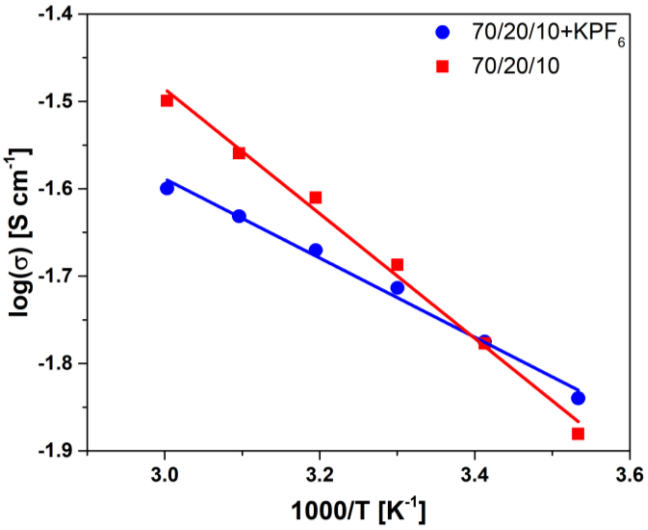

Figure 4 σ values for 70/20/10 and 70/20/10+KPF_6 electrolytes in the temperature range 10-60 °C.

Interfacial stability among potassium metal electrode and polymer membranes is a critical factor for this particular application and literature studies in the KIBs field are very limited. We investigated this aspect by assembling the GPEs between two potassium metal foils in coin cell configuration. EIS was used to follow the interface evolution and the obtained results are shown in **Figure 5**. The equivalent circuit used to fit EIS spectra and the obtained parameters are shown in **Figure S2** and **Table S1**. Charge transfer resistance (R_{Ct}), measured at low frequency, constantly increased during

test days and reached high values for the 70/20/10 formulation. This behaviour could be ascribed to the formation of an unstable spontaneous solid electrolyte interphase (SEI) layer, leading to the continuous electrolyte degradation. This fact was confirmed by the important instability of SEI layer resistance (R_{SEI}) presented in **Table S1**. A possible explanation could be the presence of some unreacted polymer precursor species in the sample, either PEGDA or BMA or even the photoinitiator, the latter free to react with metallic potassium. Such reactions seemed to be confined on the surface of potassium metal because the R_s, corresponding to the bulk resistance of polymer electrolytes, was nearly constant during days. Opposite results were obtained for the 70/20/10+KPF_6 sample. From the third testing day, R_{Ct} reached a quasi-constant value. In the meantime, R_s decreased, passing from values close to 70 to 40 Ω in the last testing days. The same behaviour was followed by R_{SEI}, constantly decreasing during test days. This trend suggested the spontaneous formation of a stable SEI layer for the 70/20/10+KPF_6 formulation. This improved interfacial stability could be explained by the K^+ cation presence in the precursor solution. Indeed, alkali cations were reported in literature for their ability to favour or even initiate radical polymerizations [53,54]; therefore, in our case K^+ could reasonably have optimized the crosslinking conditions, reducing unreacted by-products in the final GPE, thus improving the sample stability when faced to potassium. Such a poor interfacial stability of the 70/20/10 sample versus metallic potassium makes it unsuitable as a GPE, therefore all the subsequent electrochemical characterizations were performed exclusively on the 70/20/10+KPF_6 electrolyte, and the results were compared to the ones of the standard cell.

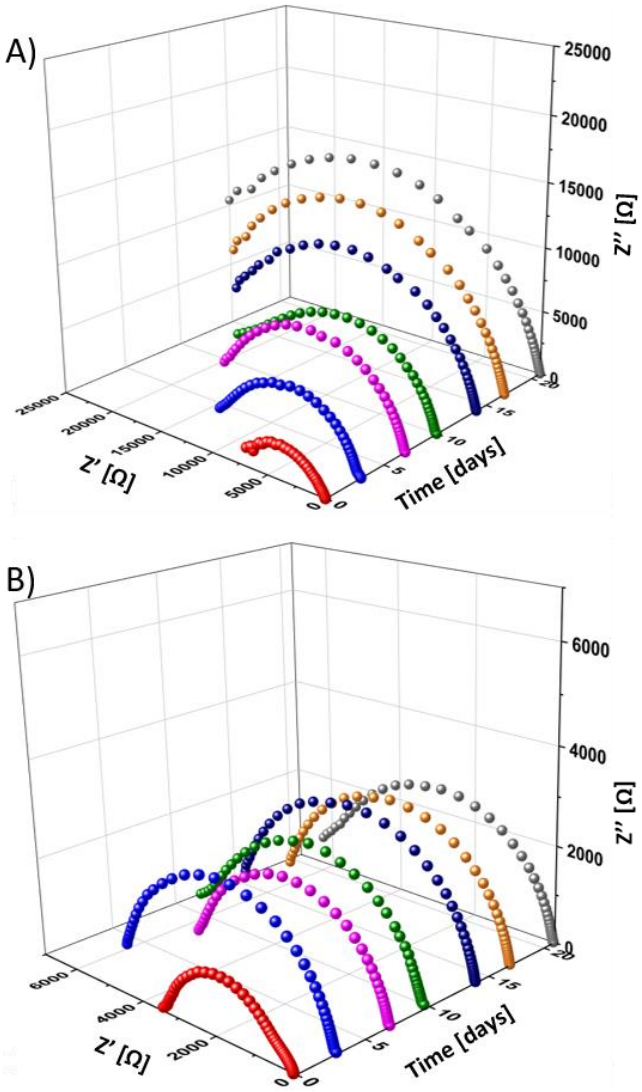

Figure 5 Interfacial stability test of A) 70/20/10 and B) 70/20/10+KPF_6 electrolytes.

To assess the electrochemical stability window of the GPE, LSV was conducted on K|GPE|SS cells in the 1-5 V interval. Eventual anodic current appearing in the current-voltage curve would in fact demonstrate the decomposition of the GPE through electrochemical oxidation. As shown in **Figure 6**, the 70/20/10+KPF_6 electrolyte exhibited no reaction up to 3.7 V *vs.* K^+/K, maintaining excellent stability within the cell working potential. The standard cell followed a similar behaviour with the same degradation onset, but the peak was shifted at higher potential involving higher current than the 70/20/10+KPF_6 electrolyte.

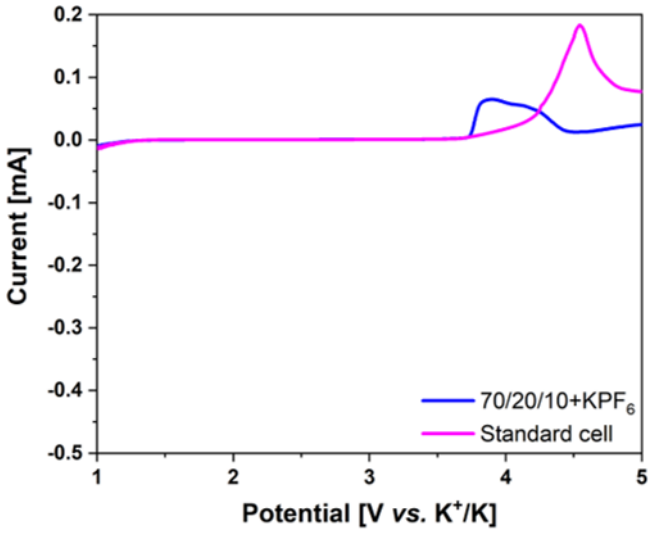

Figure 6 LSV traces of 70/20/10+KPF_6 and standard electrolytes, recorded in K|GPE|SS cells in the 1-5 V interval and at 0.1 mV s^{-1}.

Electrochemical reactions that occurred in half-cell configuration were studied by CV within the operative potential 0.01-3 V. The 70/20/10+KPF_6 electrolyte showed good reversibility starting from the second cycle, while the first cathodic scan of the voltammogram was characterized by important reactivity, as shown in **Figure 7A**. Reduction reactions could be caused by the degradation of the liquid electrolyte. In particular, EC/DEC solvent mixture can react with potassium metal anode, leading to the creation of a thick SEI layer [33], and DEC is unstable at low potential [55]. However, KPF_6 salt has a lower LUMO level and it is more prone to reduction than EC/DEC solvents in cathodic scan [56]. The subsequent cycles were reversible with almost the same path. A slope change of the curves is underlined between 0.5 and 0.8 V and could be ascribed to the insertion of potassium ions in Super P carbon. The anodic scan showed a large peak at 0.6-0.7 V caused by potassium ions de-insertion from Super P carbon [57]. No further reactions were observed at higher potential. CV plot of the standard cell (see **Figure 7B**) also showed important reduction reactions during the first cathodic scan. Based on the position of peaks and inflection points (these latter being between 1-1.25 V and 0.75-1 V; peaks being between 0.5-0.75 V and 0.25-0.5 V), the same types of reactions were occurring during the first cycle for both the GPE and the standard electrolyte. This confirms the decomposition of the liquid electrolyte and the formation of SEI layer, in accordance with previous

work [57]. The similar profiles obtained from both cells, from the 2nd cycle on, further demonstrate the electrochemical stability of the GPE upon cycling, confirming its suitability for this application.

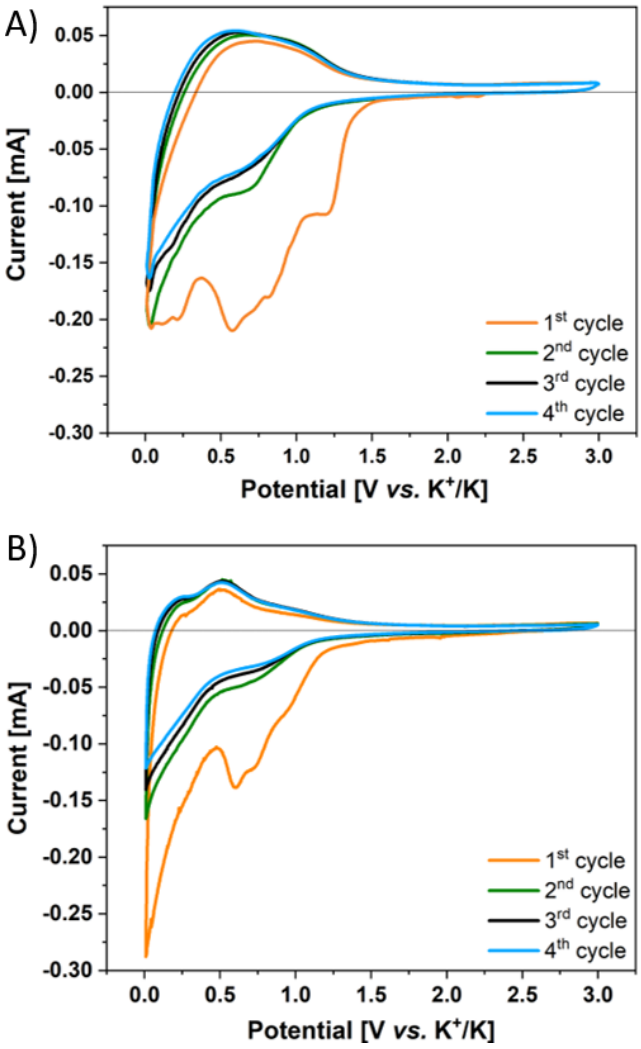

Figure 7. CV curves (recorded between 0.01 and 3 V at 0.1 mV s^{-1}) for A) 70/20/10+KPF_6 electrolyte and B) standard cell.

The ability of the selected GPE to limit dendrites growth was assessed following the potential of symmetric cells constantly charged until a short-circuit occurred. A comparison of the resulting curves can be seen in **Figure S3**. The 70/20/10+KPF_6 electrolyte was able to sustain the charge for nearly 230 h before short circuiting. In the case of the standard cell, the potential curve was initially more stable, but a short-circuit happened after only 37 h, demonstrating the scarce resistance of commercial glass fiber separator towards dendrites. In the meantime, our newly conceived electrolyte, thanks to its highly crosslinked structure, showed a better behaviour when blocking dendrites growth,

demonstrating a lifetime six times longer than the standard cell. Good performances were assessed during the plating and stripping test carried out at low current density (0.05 mA cm^{-2}), as shown in **Figure 8A**. The overpotentials are low and remain symmetric during cycles, indicating the formation of a stable interface between K metal and the GPE. Increasing the current density to 0.1 mA cm^{-2} led to a higher overpotential among the electrodes, but the robustness of the highly crosslinked membrane ensured no short-circuit occurrence between the electrodes. Further investigations could be still done to increase the cyclability of the GPE at higher current density values and by tuning the macromolecular structure to accommodate an even higher amount of liquid electrolyte; these activities will be taken into consideration in future works.

Galvanostatic charge/discharge tests were performed in half-cell configuration at room temperature to evaluate the electrochemical performance of the GPE in comparison to a standard cell. Specific capacity *vs.* cycle number plots are shown in **Figure 8BC**. In the first 100 cycles, cells were tested at different current densities from 0.05 to 1 A g^{-1} to evaluate the rate capability of the prepared cells. Following cycles were performed at 0.05 A g^{-1}. A low Coulombic efficiency was observed in the first 50 cycles for both cells, indicating important reactions between electrolyte and electrodes, probably at least partially caused by SEI formation, and already documented in a previous work [57]. A comparison of specific charge capacity expressed during the rate capability test of the GPE-based device and the standard cell are summarized in **Table 1**, demonstrating a slightly lower capacity of the GPE cell. After 200 cycles, the 70/20/10+KPF_6 electrolyte-based cell showed a specific capacity of 113 mAh g^{-1}, while the standard cell assembled with a glass fiber separator achieved a specific capacity of 156 mAh g^{-1}. However, the standard cell rapidly failed in the subsequent cycles probably for the formation of critical length dendrites short-circuiting the cell, while the GPE-based cell was able to reach 600 cycles with a final capacity retention of 58%. Of note, after the cycles series carried out at a current of 1 A g^{-1}, the capacity is fully recovered when the current of 0.05 A g^{-1} is restored; moreover, the Coulombic efficiency is always better for the GPE-based cell with respect to the standard counterpart.

These results, obtained at room temperature and with a simple lab-scale architecture, clearly confirmed the ability of the 70/20/10+KPF_6 GPE to reduce dendrite formation, thus prolonging the cycle life of the cell and enhancing its safety. In addition, to the best of our knowledge, only four papers (listed in **Table S2**) have been published up to now reporting polymer-based electrolyte for KIBs, and none of them reported the use of a UV-cured polymer matrix, the latter representing a noteworthy approach towards stable, scalable and reliable KIBs. The performances of the cells studied in the mentioned papers are summarized in **Table S2** and the maximum number of cycles reported so far is 200, thus placing our work in a leading position in terms of cycle life.

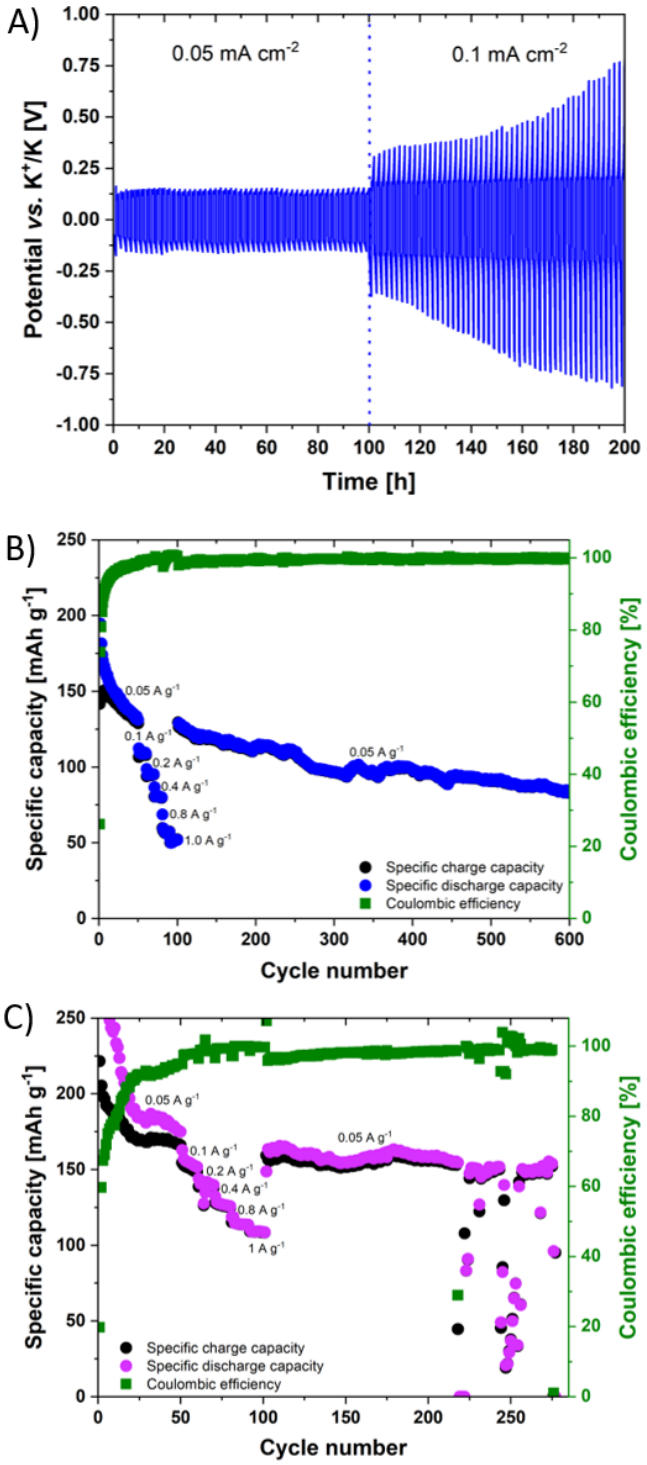

Figure 8. A) Plating and stripping test carried out on a symmetrical K/GPE/K cell at 0.05 and 0.1 mA cm^{-2}. Galvanostatic charge/discharge curves for potassium metal cells assembled with B) 70/20/10+KPF_6 electrolytes and C) standard electrolyte.

Table 1 Comparison between specific charge capacity values obtained from the GPE-based and standard cells.

Current [A g^{-1}] / Cycle	**Standard cell [mAh g^{-1}]**	**70/20/10+KPF_6 [mAh g^{-1}]**
0.05 / 50th	166	129
0.1 / 60th	149	108

0.2 / 70th	138	94.9
0.4 / 80th	125	79.8
0.8 / 90th	114	57.5
1 / 100th	108	52.2

4. Conclusions

For the first time, an UV-induced free radical polymerization approach was used to fabricate GPEs for KIBs application. Two different formulations were prepared through the copolymerization of BMA and PEGDA. The 70/20/10 formulation presented a small quantity of EC, while in the 70/20/10+KPF_6 system a small quantity of liquid electrolyte was added. The two membranes showed similar T_g values, thermal resistance and σ, but an important reactivity with potassium metal was detected for the first one. The 70/20/10+KPF_6 electrolyte, more stable against metal counter electrode, was further investigated by electrochemical techniques. The stability window of the GPE was larger than the operative potential interval of the cells and the proven ability limit suppress dendrite formation thanks to the crosslinked polymer matrix demonstrated a lifetime six times longer than the standard cell, under constant charging current. Such outstanding properties improved the cycling life, in half cell configuration and at room temperature, up to 600 cycles with a 58% capacity retention. These results aim to shed light on the field of KIBs as a promising technology for stationary energy storage.

Data availability statement

The raw/processed data required to reproduce these findings can be shared upon request to the corresponding authors

Declaration of competing interest

The authors declare that they have no known competing financial interests or personal relationships that could have appeared to influence the work reported in this paper.

References

[1] H. Zhang, B. Chen, Y. Li, J. Geng, C. Li, W. Zhao, H. Yan, Research on medium- and long-term electricity demand forecasting under climate change, *Energy Rep*. **8** (2022) 1585-1600.

[2] S. Venghaus, M. Henseleit, M. Belka, The impact of climate change awareness on behavioral changes in Germany: changing minds or changing behavior?, *Energy Sustainability Soc.* **12** (2022) art. no. 8.

[3] W. T. Wang, P. Chen, C. H. Chiang, T. F. Guo, C. G. Wu, S. P. Feng, Synergistic reinforcement of built-in electric fields for highly efficient and stable perovskite photovoltaics, *Adv. Funct. Mater.* **30** (2020) art. no. 1909755.

[4] D. Gao, L. Yang, X. Ma, X. Shang, C. Wang, M. Li, X. Zhuang, B. Zhang, H. Song, J. Chen, C. Chen, Passivating buried interface with multifunctional novel ionic liquid containing simultaneously fluorinated anion and cation yielding stable perovskite solar cells over 23% efficiency, *J. Energy Chem*. **69** (2022) 659-666.

[5] S. N. F. Yusuf, S. R. Majid, R. Yahya, Addition of 1-butyl-3-methylimidazolium iodide to the N-phthaloylchitosan based gel polymer electrolyte, *Mater. Today: Proc*. **17** (2019) 416-423.

[6] S. Akin, N. Arora, S. M. Zakeeruddin, M. Grätzel, R. H. Friend, M. I. Dar, New Strategies for Defect Passivation in High-Efficiency Perovskite Solar Cells, *Adv. Energy Mater*. **10** (2020) art. no. 1903090.

[7] C. Deng, C. Ma, M. L. Lau, P. Skinner, Y. Liu, W. Xu, H. Zhou, Y. Ren, Y. Yin, B. Williford, M. Dahl, H. C. Xiong, Amorphous and crystalline TiO_2 nanoparticle negative electrodes for sodium-ion batteries, *Electrochim. Acta* **321** (2019) art. no. 134723.

[8] J. F. Vélez, M. B. Vázquez-Santos, J. M. Amarilla, B. Herradón, E. Mann, C. del Río, E. Morales, Geminal pyrrolidinium and piperidinium dicationic ionic liquid electrolytes. Synthesis, characterization and cell performance in $LiMn_2O_4$ rechargeable lithium cells, *J. Power Sources* **439** (2019) art. no. 227098.

[9] E. K. Jang, J. Ahn, S. Yoon, K. Y. Cho, High Dielectric, Robust composite protective layer for dendrite-free and $LiPF_6$ degradation-free lithium metal anode, *Adv. Funct. Mater*. **29** (2019) art. no. 1905078.

[10] S. V. Gopinadh, P. V. R. L. Phanendra, B. John, T. D. Mercy, Fluoride-ion batteries: state-of-the-art and future perspectives, *Sustain. Mater. Technol.* **32** (2022) art. no. e00436.

[11] T. T. Tung, M. Moussa, K. M. Tripathi, T. Kim, M. J. Nine, A. K. Nanjundan, D. Dubal, D. Losic, Coupling graphene microribbons with carbon nanofibers: new carbon hybrids for high-performing lithium and potassium-ion batteries, *Sustain. Mater. Technol.* **32** (2022) art. no. e00393.

[12] J. Wang, C. Li, D. Chen, C. Sun, Z. Yang, Interlayered MoS_2/rGO thin film for efficient lithium storage produced by electrospray deposition and far-infrared reduction, *Appl. Surf. Sci*. **499** (2020) art. no. 143940.

[13] Y. Zhou, Y. Yang, N. Zhou, R. Li, Y. Zhou, W. Yan, Four-armed branching and thermally integrated imidazolium-based polymerized ionic liquid as an all-solid-state polymer electrolyte for lithium metal battery, *Electrochim. Acta* **324** (2019) art. no. 134827.

[14] X. Cai, B. Cui, B. Ye, W. Wang, J. Ding, G. Wang, Poly(ionic liquid)-based quasi-solid-state copolymer electrolytes for dynamic-reversible adsorption of lithium polysulfides in lithium-sulfur batteries, *ACS Appl. Mater. Interfaces* **11** (2019) 38136-38146.

[15] M. A. A. M. Abdah, M. Mokhtar, L. T. Khoon, K. Sopian, N. A. Dzulkurnain, A. Ahmad, Y. Sulaiman, F. Bella, M. S. Su'ait, Synthesis and electrochemical characterizations of poly(3,4-ethylenedioxythiophene/manganese oxide coated on porous carbon nanofibers as a potential anode for lithium-ion batteries, *Energy Rep.* **7** (2021) 8677-8687.

[16] D. Larcher, J. M. Tarascon, Towards greener and more sustainable batteries for electrical energy storage, *Nat. Chem*. **7** (2015) 19-29.

[17] A. Manthiram, A reflection on lithium-ion battery cathode chemistry, *Nat. Commun*. **11** (2020) art. no. 1550.

[18] X. Wang, G. M. A. Girard, H. Zhu, R. Yunis, D. R. Macfarlane, D. Mecerreyes, A. J. Bhattacharyya, P. C. Howlett, M. Forsyth, Poly(ionic liquid)s/electrospun nanofiber composite polymer electrolytes for high energy density and safe Li metal batteries, *ACS Appl. Energy Mater*. **2** (2019) 6237-6245.

[19] K. Xu, A long journey of lithium: from the Big Bang to our smartphones, *Energy Environ. Mater*. **2** (2019) 229-233.

[20] X. Zhang, L. Duan, X. Zhang, X. Li, W. Lü, Preparation of Cu_2S@rGO hybrid composites as anode materials for enhanced electrochemical properties of lithium ion battery, *J. Alloys Compd*. **816** (2020) art. no. 152539.

[21] C. Wang, T. Wang, L. Wang, Z. Hu, Z. Cui, J. Li, S. Dong, X. Zhou, G. Cui, Differentiated lithium salt design for multilayered PEO electrolyte enables a high-voltage solid-state lithium metal battery, *Adv. Sci*. **6** (2019) art. no. 1901036.

[22] L. Wang, G. Yang, S. Peng, J. Wang, W. Yan, S. Ramakrishna, One-dimensional nanomaterials toward electrochemical sodium-ion storage applications via electrospinning, *Energy Storage Mater*. **25** (2020) 443-476.

[23] H. Zhai, B. Y. Xia, H. S. Park, Ti-based electrode materials for electrochemical sodium ion storage and removal, *J. Mater. Chem. A* **7** (2019) 22163-22188.

[24] M. S. Park, H. S. Woo, J. M. Heo, J. M. Kim, R. Thangavel, Y. S. Lee, D. W. Kim, Thermoplastic polyurethane elastomer-based gel polymer electrolytes for sodium-metal cells with enhanced cycling performance, *ChemSusChem* **12** (2019) 4645-4654.

[25] F. Bella, S. De Luca, L. Fagiolari, D. Versaci, J. Amici, C. Francia, S. Bodoardo, An overview on anodes for magnesium batteries: challenges towards a promising storage solution for renewables, *Nanomaterials* **11** (2021) art. no. 810.

[26] M. Alidoost, A. Mangini, F. Caldera, A. Anceschi, J. Amici, D. Versaci, L. Fagiolari, F. Trotta, C. Francia, F. Bella, S. Bodoardo, Micro-mesoporous carbons from cyclodextrin nanosponges enabling high-capacity silicon anodes and sulfur cathodes for lithiated Si-S batteries, *Chem. Eur.-J.* **28** (2022) art. no. e202104201.

[27] H. Gao, L. Xue, S. Xin, J. B. Goodenough, A high-energy-density potassium battery with a polymer-gel electrolyte and a polyaniline cathode, *Angew. Chem. Int. Ed*. **57** (2018) 5449-5453.

[28] J. Y. Hwang, S. T. Myung, Y. K. Sun, Sodium-ion batteries: present and future, *Chem. Soc. Rev.* **46** (2017) art. no. 3529.

[29] M. Zhou, P. Bai, X. Ji, J. Yang, C. Wang, Y. Xu, Electrolytes and interphases in potassium ion batteries, *Adv. Mater.* **33** (2021) art. no. 2003741.

[30] A. Massaro, A. B. Muñoz-García, P. Maddalena, F. Bella, G. Meligrana, C. Gerbaldi, M. Pavone, First-principles study of Na insertion at TiO_2 anatase surfaces: new hints for Na-ion battery design, *Nanoscale Adv.* **2** (2020) 2745-2751.

[31] S. Ye, L. Wang, F. Liu, P. Shi, Y. Yu, Integration of homogeneous and heterogeneous nucleation growth via 3D alloy framework for stable Na/K metal anode, *eScience* **1** (2021) 75-82.

[32] A. Eftekhari, Potassium secondary cell based on Prussian blue cathode, *J. Power Sources* **126** (2004) 221-228.

[33] Y. Liu, C. Gao, L. Dai, Q. Deng, L. Wang, J. Luo, S. Liu, N. Hu, The features and progress of electrolyte for potassium ion batteries, *Small* **16** (2020) art. no. 2004096.

[34] X. Zhang, J. Meng, X. Wang, Z. Xiao, P. Wu, L. Mai, Comprehensive insights into electrolytes and solid electrolyte interfaces in potassium-ion batteries, *Energy Storage Mater.* **38** (2021) 30-49.

[35] M. Okoshi, Y. Yamada, S. Komaba, A. Yamada, H. Nakai, Theoretical analysis of interactions between potassium ions and organic electrolyte solvents: a comparison with lithium, sodium, and magnesium ions, *J. Electrochem. Soc.* **164** (2017) art. no. A54.

[36] L. Wang, J. Yang, J. Li, T. Chen, S. Chen, Z. Wu, J. Qiu, B. Wang, P. Gao, X. Niu, H. Li, Graphite as a potassium ion battery anode in carbonate-based electrolyte and ether-based electrolyte, *J. Power Sources* **409** (2019) 24-30.

[37] X. Cheng, J. Pan, Y. Zhao, M. Liao, H. Peng, Gel polymer electrolytes for electrochemical energy storage, *Adv. Energy Mater.* **8** (2018) art. no. 1702184.

[38] X. Zhou, H. Jiang, H. Zheng, Y. Sun, X. Liang, H. Xiang, Nonflammable hybrid solid electrolyte membrane for a solid-state lithium battery compatible with conventional porous electrodes, *J. Membr. Sci.* **603** (2020) art. no. 117820.

[39] T. C. Mendes, N. Goujon, N. Malic, A. Postma, J. Chiefari, H. Zhu, P. C. Howlett, M. Forsyth, Polymerized ionic liquid block copolymer electrolytes for all-solid-state lithium-metal batteries, *J. Electrochem. Soc.* **167** (2020) art. no. 070525.

[40] J. Amici, C. Torchio, D. Versaci, D. Dessantis, A. Marchisio, F. Caldera, F. Bella, C. Francia, S. Bodoardo, Nanosponge-based composite gel polymer electrolyte for safer Li-O_2 batteries, *Polymers* **13** (2021) art. no. 1625.

[41] H. Fei, Y. Liu, Y. An, X. Xu, G. Zeng, Y. Tian, L. Ci, B. Xi, S. Xiong, J. Feng, Stable all-solid-state potassium battery operating at room temperature with a composite polymer electrolyte and a sustainable organic cathode, *J. Power Sources* **399** (2018) 294-298.

[42] J. Zheng, L. Schkeryantz, G. Gourdin, L. Qin, Y. Wu, Single potassium-ion conducting polymer electrolytes: preparation, ionic conductivities, and electrochemical stability, *ACS Appl. Energy Mater.* **4** (2021) 4156-4164.

[43] F. Colò, F. Bella, J. R. Nair, C. Gerbaldi, Light-cured polymer electrolytes for safe, low-cost and sustainable sodium-ion batteries, *J. Power Sources* **365** (2017) 293-302.

[44] X. Zhao, C. Tao, Y. Li, X. Chen, J. Wang, H. Gong, Preparation of gel polymer electrolyte with high lithium ion transference number using GO as filler and application in lithium battery, *Ionics* **26** (2020) 4299-4309.

[45] P. Xu, H. Chen, X. Zhou, H. Xiang, Gel polymer electrolyte based on PVDF-HFP matrix composited with rGO-PEG-NH_2 for high-performance lithium ion battery, *J. Membr. Sci*. **617** (2021) art. no. 118660.

[46] A. Arya, A. L. Sharma, Polymer electrolytes for lithium ion batteries: a critical study, *Ionics* **23** (2017) 497-540.

[47] Y. Guo, S. Wu, Y. B. He, F. Kang, L. Chen, H. Li, Q. H. Yang, Solid-state lithium batteries: safety and prospects, *eScience* **2** (2022) 138-163.

[48] K. Suhailath, M. T. Ramesan, B. Naufal, P. Periyat, V. C. Jasna, P. Jayakrishnan, Synthesis, characterisation and flame, thermal and electrical properties of poly (n-butyl methacrylate)/titanium dioxide nanocomposites, *Polym. Bull.* **74** (2017) 671-688.

[49] M. Begum, Siddaramaiah, Synthesis and characterization of polyurethane/polybutyl methacrylate interpenetrating polymer networks, *J. Mater. Sci.* **39** (2004) 4615-4623.

[50] S. Ray, R. P. Cooney, Chapter 9 - Thermal degradation of polymer and polymer composites, *Handbook of Environmental Degradation of Materials (Third Edition)* (2018) 185-206.

[51] H. Yin, C. Han, Q. Liu, F. Wu, F. Zhang, Y. Tang, Recent advances and perspectives on the polymer electrolytes for sodium/potassium-ion batteries, *Small* **17** (2021) art. no. 2006627.

[52] Z. Wu, J. Zou, S. Shabanian, K. Golovin, J. Liu, The roles of electrolyte chemistry in hard carbon anode for potassium-ion batteries, *Chem. Eng. J.* **427** (2022) art. no. 130972.

[53] M. Xie, Y. Wu, Y. Liu, P. P. Yu, R. Jia, W. A. Goddard, T. Cheng, Pathway of *in situ* polymerization of 1,3-dioxolane in $LiPF_6$ electrolyte on Li metal anode, *Mater. Today Energy* **21** (2021) art. no. 100730.

[54] Y. Miwa, H. Tsutsumi, T. Oishi, Polymerization of bis-oxetanes consisting of oligo-ethylene oxide chain with lithium salts as initiators, *Polym. J.* **33** (2001) 568-574.

[55] J. Zhao, X. Zou, Y. Zhu, Y. Xu, C. Wang, Electrochemical intercalation of potassium into graphite, *Adv. Funct. Mater*. **26** (2016) 8103-8110.

[56] H. Wang, H. Wang, S. Chen, B. Zhang, G. Yang, P. Gao, J. Liu, X. Fan, Y. Huang, J. Lin, Z. Shen, Depth-profiling study on the solid electrolyte interface: bis(fluorosulfuryl)imide anion toward improved K^+ storage, *ACS Appl. Energy Mater*. **2** (2019) 7942-7951.

[57] C. Zhang, Y. Xu, M. Zhou, L. Liang, H. Dong, M. Wu, Y. Yang, Y. Lei, Potassium Prussian blue nanoparticles: a low-cost cathode material for potassium-ion batteries, *Adv. Funct. Mater*. **27** (2017) art. no. 1604307.

Declaration of interests

☒ The authors declare that they have no known competing financial interests or personal relationships that could have appeared to influence the work reported in this paper.

☐The authors declare the following financial interests/personal relationships which may be considered as potential competing interests:

Author Statement

Matteo Gandolfo: Methodology; Investigation; Writing - Original Draft

Julia Amici: Conceptualization; Writing - Original Draft; Supervision

Lucia Fagiolari: Methodology; Investigation; Writing - Review & Editing

Carlotta Francia: Validation; Writing - Review & Editing

Silvia Bodoardo: Funding acquisition; Writing - Review & Editing

Federico Bella: Conceptualization; Writing - Original Draft; Supervision; Project administration